Ocean Engineering 210 (2020) 107567

Contents lists available at ScienceDirect

Ocean Engineering

journal homepage: www.elsevier.com/locate/oceaneng

Glider performance analysis and intermediate-fidelity modelling of underwater vehicles

Clemens Deutsch [a,*], Jakob Kuttenkeuler [a], Tomas Melin [b]

[a] KTH Royal Institute of Technology, Teknikringen 8, 114 28 Stockholm, Sweden
[b] Swedish Defence Research Agency, Gullfossgatan 6, 164 40 Kista, Sweden

ARTICLE INFO

Keywords:
Autonomous Underwater Vehicle (AUV)
Underwater glider
Performance
Hydrodynamic modelling

ABSTRACT

This paper analyses the transit performance of state-of-the-art underwater vehicles and presents an intermediate-fidelity steady-state flight mechanics model for qualitative performance assessment of underwater vehicles. Focusing on the comparison of underwater gliders and propeller-driven AUVs, a simple glide metric is presented and the transit performance of the legacy underwater gliders Slocum, Spray and Seaglider as well as propeller-modified versions thereof is evaluated. The evaluation is based on various data sets from wind tunnel tests and Computational Fluid Dynamics (CFD) studies, and shows that for the respective hull shapes gliding locomotion proves more efficient in ideal conditions. However, biofouling conditions inflict a double penalty on glider performance, rendering gliders inferior to propeller-driven vehicles. The Slocum data set is used to validate a steady-state flight mechanics model for qualitative performance prediction. It is shown that even simplistic models based on semi-empirical and analytical expressions can be successfully used for design optimization through parametrization. Being computationally efficient, the model can be a useful tool for design engineers in early design phases. The model is used to evaluate the effects of wing span on gliding efficiency, indicating that the current design of the Slocum glider is near-optimal.

1. Introduction

In times of global climate change there is a significantly increasing interest among the oceanographic community in pushing boundaries and shedding light into the great vastness of yet unexplored regions in our oceans — which play a vital role in the planet's climate physics. Especially the polar waters, under and around the Antarctic ice shelf and the Arctic ice sheet, have been receiving attention in recent years (King et al., 2019; McPhail et al., 2019; Yamagata et al., 2019), imposing great challenges on engineers to improve the current generation of state-of-the-art autonomous underwater vehicles (AUVs). Long-term ocean observation and monitoring helps climate scientists understand and predict physical processes in the atmosphere better. Typical missions can extend over hundreds or even thousands of kilometres in range and last for several months. This spatial and temporal extent inevitably increases requirements towards autonomy, navigation and endurance of AUVs. The endurance of AUVs depends on two factors: Energy consumption and energy capacity (Yuh et al., 2011). Energy capacity mainly depends on battery technology and allocated size, whereas energy consumption is a function of vehicle shape, operational speed (propulsive power), and hotel load. Increasing both the temporal and spatial range of underwater vehicles enables scientists to gather more and better data at less financial expense.

For many years there has been consensus among AUV designers and operators that underwater gliders generally are superior in terms of range and endurance in comparison to common propeller-driven AUVs (Gafurov and Klochkov, 2015). Dhanak and Xiros (2016) analysed the efficiency of propeller blades and wings based on hydromechanic principles, concluding that wings are intrinsically more efficient due to their vortex shedding characteristics. However, this analysis did not consider the differences in locomotion of propeller-driven level flight and sawtooth-like glide cycles. Already in 2010, Steinberg et al. (2010) performed a study on the transit performance of both types of propulsion systems, concluding that they are equally efficient in terms of transit energy consumption, and that the choice of propulsion system ultimately should depend on the application only. In recent years, several AUVs with outstanding long-range capabilities have been presented (Furlong et al., 2007; McPhail, 2009; Furlong et al., 2012; Hobson et al., 2012; Roper et al., 2017), offering a potentially interesting alternative to underwater gliders in the domain of long-range underwater missions. The research question however, which of the propulsion systems provides the better performance for

* Corresponding author.
E-mail address: clemensd@kth.se (C. Deutsch).

https://doi.org/10.1016/j.oceaneng.2020.107567
Received 25 November 2019; Received in revised form 19 May 2020; Accepted 23 May 2020
Available online 9 June 2020

long-range horizontal travel, has not been attended to enough. In this paper, the transit performance of the legacy underwater gliders Slocum, Spray, and Seaglider as well as propeller-modified versions thereof is assessed in ideal and biofouling conditions. The evaluation is based on published computational and experimental data. A simple, yet generic intermediate-fidelity steady-state flight mechanics model for underwater vehicles is presented and validated against the published data. It is shown how the model can be applied in vehicle design optimization. In order to help engineers understand how design configurations affect vehicle performance it is most important for the model to be able to predict the hydrodynamic behaviour qualitatively correct, with acceptable quantitative accuracy.

2. Performance of underwater vehicles

Performance is a human-defined concept and as such it is dynamic; its meaning can vary between different users and operators depending on their ultimate goals or application. Here, performance is evaluated in terms of range, endurance and speed. Other definitions of performance can include manoeuvrability, autonomy or be more sensor-specific.

In the following, the theoretical background of underwater locomotion is elaborated on briefly. Since underwater gliding poses a special case in terms of locomotion, the most important flight mechanics of gliders are presented. After that, the transit performance of both underwater gliders and propeller-driven AUVs is defined. This section is concluded with a short review on the effects of marine biofouling on the hydrodynamic properties of lifting bodies — an important aspect when evaluating flight performance in real-world conditions. Throughout the paper the hydrodynamic forces drag D and lift L are expressed in terms of the dimensionless drag coefficient C_D and lift coefficient C_L, respectively,

$$D = \frac{1}{2}\rho U^2 C_D(\alpha, R_e)A, \tag{1}$$

$$L = \frac{1}{2}\rho U^2 C_L(\alpha, R_e)A. \tag{2}$$

Here, ρ is the density of the surrounding fluid (i.e. seawater), U is the inflow velocity, and A the reference area that the hydrodynamic coefficients are referenced to. Both hydrodynamic coefficients can be functions of the angle of attack α and the Reynolds number Re.

2.1. Gliding locomotion

Underwater gliders glide along an inclined trajectory by alternating between positive and negative net buoyancy B_{net} as schematically shown in Fig. 1. The lifting surfaces generate a lift force that is responsible for horizontal travel of the vehicle. The angle of attack α and the inflow velocity determine hydrodynamic drag and lift acting on the vehicle. The instantaneous angle of attack on the vehicle can be controlled by moving an internal mass and hence changing the vehicle's attitude. The ratio of the hydrodynamic forces also determines the glide path angle γ as

$$\gamma = \tan^{-1}\frac{C_D}{C_L}. \tag{3}$$

From conservation of mechanical energy the following expressions for vertical velocity w (also known as sink rate) and horizontal velocity u can be derived as (Wagner, 2003; Dhanak and Xiros, 2016)

$$u = \sqrt{\frac{2B_{net}}{\rho A}}\frac{C_L(\alpha, R_e)}{\left(C_L^2(\alpha, R_e) + C_D^2(\alpha, R_e)\right)^{3/4}}, \tag{4}$$

$$w = \sqrt{\frac{2B_{net}}{\rho A}}\frac{C_D(\alpha, R_e)}{\left(C_L^2(\alpha, R_e) + C_D^2(\alpha, R_e)\right)^{3/4}}. \tag{5}$$

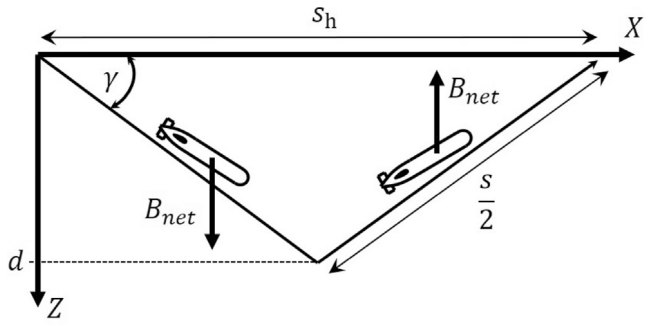

Fig. 1. Gliding locomotion of underwater gliders in a global reference frame denoted by the horizontal axis X and vertical axis Z. The origin is located in the water surface where the dive cycle is initiated. The glider glides to apogee depth d due to negative net buoyancy B_{net} and surfaces again due to positive net buoyancy. The travelled distance along the glide path angle γ is s, and the respective transit distance is s_h.

2.2. Transit efficiency and glide metric

The transit efficiency is evaluated in terms of the energy required per metre (horizontal travel) and denoted by E_T in joule per metre. For the propeller-driven AUV (superscript P) the energy required per metre is equal to the drag force D,

$$E_T^P = \frac{Ds}{s} = D. \tag{6}$$

For the glider (superscript G) it can be seen from Fig. 1 that the travelled transit distance s_h is inversely proportional to the tangent of the glide path angle and directly proportional to the apogee depth d, yielding

$$s_h = \frac{2d}{\tan\gamma}. \tag{7}$$

The effective pump energy E_P expended at apogee depth d is

$$E_P = B_{net}d. \tag{8}$$

Assuming negligible pump energy consumption to initiate a dive cycle, (7) and (8) can now be combined to obtain the glider's energy consumption per metre travelled horizontally (per dive cycle) as

$$E_T^G = \frac{1}{2}B_{net}\tan\gamma = \frac{1}{2}B_{net}\frac{C_D}{C_L}. \tag{9}$$

Here, it also is assumed that the time required to reach terminal velocity (steady state) is much smaller than the total time of a dive cycle, i.e. the acceleration phase does not affect the transit efficiency. When estimating the achievable range for a given vehicle configuration, energy consumption from propulsion as well as all other on-board systems, e.g. scientific instrumentation, needs to be included. It therefore is more practical to study propulsive power rather than energy consumption. For the propeller-driven AUV the propulsive power P_p is the effective power needed to overcome drag, and is expressed as

$$P_p^P = \frac{1}{2}\rho U^3 C_D A\frac{1}{\eta_p^P} \tag{10}$$

where the propulsive efficiency η_p^P for the propeller-based powertrain is introduced. For the underwater glider, the equivalent propulsive power P_p^G (averaged over one dive-cycle) for the transit case is given as

$$P_p^G = \frac{1}{2}\rho u^3 C_{GL} A\frac{1}{\eta_p^G}, \tag{11}$$

where η_p^G is the efficiency of the buoyancy system and C_{GL} denotes the glide coefficient. Its dependency on C_D and C_L is derived from (4) and (9) by substituting the net buoyancy-term as

$$C_{GL} = \frac{C_D(C_D^2 + C_L^2)^{3/2}}{2C_L^3}. \tag{12}$$

In cases where C_D and C_L are Re-independent and only a function of α, the optimum angle of attack that enables maximum range can be identified by finding the simple zero of the derivative of the glide coefficient with respect to α. By taking the ratio of P_p^G/P_p^P, a simple design metric (referred to as the *glide metric*) for the determination of a favourable propulsion system is derived. The underwater glider thus is considered more efficient in transit when the following inequality is satisfied

$$\frac{C_D(C_D^2+C_L^2)^{3/2}}{2C_{D0}C_L^3} < \frac{\eta_p^G}{\eta_p^P}, \tag{13}$$

where C_{D0} represents the reference drag coefficient at zero angle of attack. Ideally, the reference drag coefficient is taken as the bare hull drag coefficient, enabling comparison between underwater glider and propeller-driven AUV. However, for small wings the drag contribution can be argued to be negligible since the wing surface area is significantly smaller than the wetted surface area of the body. From an engineering perspective, the propulsive efficiency of the buoyancy engine is hard to evaluate. The efficiency of buoyancy engines can vary significantly from 8 % to 70 %, depending on operating pressure and the actual technology used (Rudnick et al., 2004; Kobayashi et al., 2010; Worall et al., 2007), whereas the propulsive efficiency of propeller-based powertrains averages at about 50 % (Furlong et al., 2007; Phillips et al., 2012). Therefore, the ratio η_p^P/η_p^G is neglected in the performance evaluation in Section 4, i.e. assumed to be equal to 1. Due to the glider's complex dynamics, physical interpretation of metrics such as (13) often is rather cumbersome despite their conceptually simple derivation. Chen et al. (2015) and Fu et al. (2018) have applied a similar metric based on a power conversion principle (power consumption in the horizontal direction compared to net buoyancy potential output). The benefit of using (13) is its sole dependency on hydrodynamic coefficients and therefore simple integration in the design process.

2.3. Effects of marine biofouling

Hydrodynamic coefficients are often computed only for ideal conditions, assuming smooth surfaces for the vehicle and all appendices. However, especially on long-endurance missions this assumption is likely to be violated by the formation of marine biofouling. Marine biofouling is caused by the adhesion and growth of marine animals, plants, and slime on the surface of a submerged body and can significantly decrease the operational efficiency of underwater vehicles. The type and intensity of biofouling strongly depends on environmental variables such as water quality, temperature, currents and sunlight conditions (Lobe et al., 2010; Orme et al., 2001). First traces of biofouling can be seen after just a few weeks of operation, and in the worst case render the vehicle inoperative within three months of operation (Haldeman et al., 2016). Even though the negative effects of marine biofouling are well known to the maritime community, its effects on vehicle performance, in particular with respect to different propulsion systems, are yet to be studied. While propeller-driven vehicles mostly suffer from increased drag, underwater gliders suffer from increased drag and simultaneously decreased lift. Results from experimental (Orme et al., 2001) and numerical (Khor and Xiao, 2011) studies on lifting bodies are in fairly good agreement with the results published by Walker et al. (2014), suggesting a decrease in lift coefficient by up to ≈40 % and an increase in drag coefficient by up to ≈90 % for medium to severe levels of biofouling. In accordance, the hydrodynamic coefficients are corrected for biofouling by applying penalty factors. The equations for biofouling-corrected drag and lift coefficients C_D^{bf} and C_L^{bf}, respectively, then read

$$C_D^{bf} = 1.9 \cdot C_D, \tag{14}$$

$$C_L^{bf} = 0.6 \cdot C_L. \tag{15}$$

3. Numerical modelling

A simple, yet generic steady-state model for flight mechanics of underwater vehicles is derived from force balance using analytical as well as semi-empirical expressions for hydrodynamic estimates. The model is valid for both propeller-driven AUVs and underwater gliders. The applicability and usefulness of similar simple models has been proven in the past (Nahon, 1996; Furlong et al., 2007). When using such models, it is of uttermost importance to understand the limitations imposed by the model itself in order to interpret output thereof. Fig. 2 shows forces, angles and coordinate systems in a free-body diagram. The model is constrained to the xz-plane (dive plane), hence only 3 degrees of freedom (DOF) are considered: surge, heave and pitch. The AUV is modelled in a body-fixed coordinate system and an earth-fixed coordinate system using Cartesian coordinates. All forces and their positions are expressed in the body-fixed coordinate system. The origin of the body-fixed coordinate system is chosen as the stern of the hull.

Exemplarily, the AUV is divided into three sections: body, wings and (tail) fins. These sections are referred to by subscripts b, w and t, respectively. However, the model is easily modifiable and can be adjusted to other subdivisions. The centre of pressure of each section is described by its longitudinal and, if applicable, vertical positions (i.e. $x_{b/w/t}$ and $z_{b/w/t}$), and is considered to be constant for all flight conditions. This is one of the major simplifications and yet a necessary sacrifice of solution accuracy in order to achieve reasonably fast computation. The same assumption is applied to the centre of buoyancy C_B and the centre of gravity C_G. Their locations are defined by their vertical (z) and longitudinal (x) coordinates with subscripts B and G, respectively. The chord lengths of the control surfaces (wing and tail) are denoted by c, and their deflection by δ, with corresponding subscripts. The thrust force T is applied at the respective x- and z-location x_T and z_T. Optionally, vectored thrust can be implemented into the model by considering the thrust vector angle δ_T. Interference effects between thrusters and hull or control surfaces are neglected, e.g. increased elevator lift due to locally increased pressure in the propeller slipstream. The angle between the coordinate systems is the pitch angle ϕ, see Fig. 2. The slope angle (or glide-path angle, see (3)) γ is defined as the direction of travel relative to the horizontal axis and the vehicle speed along γ is the absolute velocity U. Pitch angle and slope angle are coupled through the angle of attack α as

$$\phi = \alpha + \gamma. \tag{16}$$

The angle of attack is assumed to be constant over the entire vehicle. The hydrodynamic force along the axis of motion is drag D, the hydrodynamic force perpendicular to that is lift L. Lift and drag are calculated separately for each vehicle section. The buoyancy force B is acting positively upwards through C_B and the gravity force G is acting positively downward through C_G. The difference between B and G is the net buoyancy. For static equilibrium in the body-fixed coordinate system (around origin) the following three equations must be satisfied:

$$\sum F_x : \begin{pmatrix} B-G \\ T \end{pmatrix}^{\mathrm{T}} \begin{pmatrix} \sin\phi \\ \cos\delta_T \end{pmatrix} + \begin{pmatrix} 1 \\ 1 \\ 1 \end{pmatrix}^{\mathrm{T}} \begin{bmatrix} L_b & D_b \\ L_w & D_w \\ L_t & D_t \end{bmatrix} \begin{bmatrix} \sin\alpha \\ -\cos\alpha \end{bmatrix} = 0, \tag{17}$$

$$\sum F_z : \begin{pmatrix} B-G \\ T \end{pmatrix}^{\mathrm{T}} \begin{pmatrix} -\cos\phi \\ -\sin\delta_T \end{pmatrix} - \begin{pmatrix} 1 \\ 1 \\ 1 \end{pmatrix}^{\mathrm{T}} \begin{bmatrix} L_b & D_b \\ L_w & D_w \\ L_t & D_t \end{bmatrix} \begin{bmatrix} \cos\alpha \\ \sin\alpha \end{bmatrix} = 0, \tag{18}$$

$$\sum M_y : \begin{pmatrix} B \\ -G \end{pmatrix}^{\mathrm{T}} \begin{bmatrix} x_B & z_B \\ x_G & z_G \end{bmatrix} \begin{pmatrix} \cos\phi \\ \sin\phi \end{pmatrix} + \begin{pmatrix} x_b \\ x_w \\ x_t \end{pmatrix}^{\mathrm{T}} \begin{bmatrix} L_b & D_b \\ L_w & D_w \\ L_t & D_t \end{bmatrix} \begin{bmatrix} \cos\alpha \\ \sin\alpha \end{bmatrix} + M_{oc} + M_T = 0. \tag{19}$$

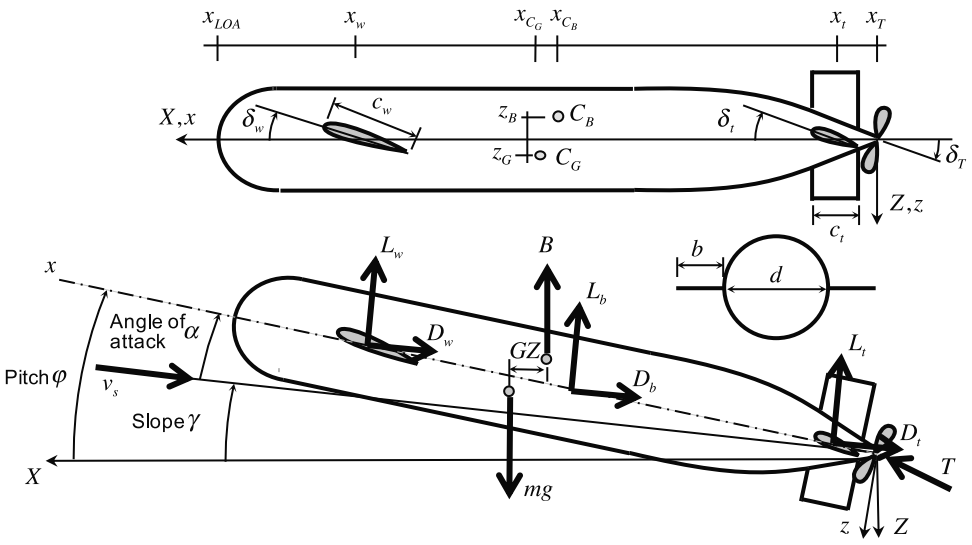

Fig. 2. The AUV in the body-fixed (xz) and earth-fixed (XZ) coordinate systems. (Top) Important distances and angles. (Bottom) Forces acting on the AUV.

The last two terms in (19) represent moments caused by off-centreline hydrodynamic forces (for which $z_i \neq 0$) as well as moments caused by vectored thrust when it is applied elsewhere than in the origin. The off-centreline moments M_{oc} are given by

$$M_{oc} = \begin{pmatrix} z_b \\ z_w \\ z_t \end{pmatrix}^{\mathrm{T}} \begin{bmatrix} L_b & D_b \\ L_w & D_w \\ L_t & D_t \end{bmatrix} \begin{bmatrix} \sin\alpha \\ \cos\alpha \end{bmatrix} \tag{20}$$

and the thrust vectoring moment M_T is given by

$$M_T = \begin{pmatrix} x_T \\ z_T \end{pmatrix}^{\mathrm{T}} T \begin{pmatrix} \sin\delta_T \\ \cos\delta_T \end{pmatrix}. \tag{21}$$

The hydrodynamic forces that appear in (17)–(20) are calculated separately for each source of origin. This model considers frictional drag, lift and lift-induced drag. For simplification, the dynamic pressure q is defined beforehand as

$$q = \frac{1}{2}\rho U^2. \tag{22}$$

3.1. Forces on the body

The buoyancy force B is defined as

$$B = \rho g V, \tag{23}$$

where g is the gravitational constant and V is the volume displaced by the vehicle. The gravity force G is the product of vehicle dry mass m and the gravitational constant g,

$$G = mg. \tag{24}$$

It is assumed that the AUV is a streamlined body, thus neglecting form drag and only considering friction drag and lift-induced drag. Furthermore, wave drag is neglected assuming operation at sufficiently large water depths. The body friction drag D_{bf} is calculated as

$$D_{bf} = qC_f A_{wet}. \tag{25}$$

Here, A_{wet} is the reference area which in case of friction drag is the wetted surface area. C_f is the frictional drag coefficient which has to be determined depending on the governing flow regime. The flow regime generally is characterized by the Reynolds number Re (Schlichting et al., 2016) which is a function of the specific length L, the inflow velocity U and the kinematic viscosity ν of the surrounding fluid (here $\nu = 1 \times 10^{-6}\ \mathrm{m^2\ s^{-1}}$),

$$Re = \frac{LU}{\nu}. \tag{26}$$

The Reynolds number determines whether the flow is laminar, turbulent or in the transition region in between. Turbulent flow develops at higher Reynolds numbers but can also be caused by e.g. by surface roughness and vortex-shedding edges. A simple but common approach is to identify a critical Reynolds number at which the flow switches from laminar to turbulent. This critical Reynolds number often is assumed to be 550 000 (Schlichting et al., 2016). Transition effects are difficult to model and the interested reader is referred to Lidtke et al. (2019) for a deeper analysis of transition effects on underwater gliders. The frictional drag coefficient in the turbulent case ($Re > 550000$) is estimated from Prandtl's one-seventh-power law (Prandtl, 1925)

$$C_{f,\mathrm{turbulent}} = \frac{0.027}{Re^{1/7}} \tag{27}$$

and for the laminar case from Blasius' skin friction line (Phillips et al., 2017)

$$C_{f,\mathrm{laminar}} = \frac{1.327}{Re^{1/2}} \tag{28}$$

Additionally, it is recommended to increase the frictional drag coefficient by the form factor k (Joung et al., 2012; Phillips et al., 2017). For spheroids Hoerner (1965) suggests multiplication with the following expression

$$(1+k) = 1 + 1.5\left(\frac{2r}{L}\right)^{\frac{3}{2}} + 7\left(\frac{2r}{L}\right)^{3} \tag{29}$$

where L, as previously, is the vehicle length and $2r$ is the nominal vehicle diameter.

When the AUV is moving with a non-zero α the vehicle body generates hydrodynamic lift L_b and lift-induced drag D_{bi}. The angle of attack is assumed constant over the hull length. These forces are estimated as (Hoerner, 1965)

$$L_b = qC_L \frac{A_{wet}}{\pi}, \tag{30}$$

$$D_{bi} = qC_{Di} \frac{A_{wet}}{\pi}. \tag{31}$$

Here, C_L and C_{Di} are the coefficients of lift and lift-induced drag, respectively. The reference area in (31) and (30) still is the wetted surface area. Scaling with $1/\pi$ is necessary in order to stay consistent with Hoerner (1965). The coefficients for lift and lift-induced drag are also estimated from (Hoerner, 1965):

$$C_{Di} = C_d \sin^3\alpha. \tag{32}$$

$$C_L = C_d \sin^2\alpha \cos\alpha. \tag{33}$$

In (32) and (33) C_d is the two-dimensional drag coefficient, here assumed to be ≈1.1 for bodies of revolution, which is the drag coefficient for a 2D cylinder. The total body drag is

$$D_b = D_{bf} + D_{bi}. \tag{34}$$

3.2. Forces on control surfaces

The forces on the control surfaces, i.e. wings and tail fins/rudders, are modelled similarly to the body forces. All control surfaces are approximated as rectangular, not swept and not twisted surfaces with constant cross-section over the whole wing span. The lift and drag forces are calculated as

$$L_{t,w} = qC_L A_p, \tag{35}$$

$$D_{t,w} = qC_D A_p. \tag{36}$$

It shall be noted that the reference area changes in comparison to (31) and (30). In (35) and (36) the reference area is the wing planform area A_p (Hoerner, 1965), and due to the assumptions made it is the product of wing span and chord length. The three-dimensional lift coefficient is given as (Torenbeek and Wittenberg, 2009)

$$C_L = \frac{C_l}{1 + \frac{2}{eAR}}. \tag{37}$$

Here, AR is the aspect ratio of the control surface and e is the span efficiency (also known as Oswald efficiency number). In practice, this value often is taken as ≈0.9 although its true value is strictly design-dependent and can be significantly lower (Sadraey, 2017). C_l is the two-dimensional lift-coefficient for the control surface, computed as

$$C_l = C_{l\alpha}(\alpha + \delta). \tag{38}$$

Here, $C_{l\alpha}$ is the lift curve slope and assumed to be equal to 2π, which can be derived from vortex theory for thin aerofoils of infinite span in incompressible flow (Torenbeek and Wittenberg, 2009). The surface deflection δ needs to be added to the angle of attack in order to consider the local angle of attack. Body-wing interference usually is negligible for large wing-span-to-body-diameter ratios (b/d). Unfortunately, most underwater gliders have relatively small b/d-ratios (e.g. typically ≈3 for underwater gliders, ≈13 for aerial gliders) and hence body-wing interference has to be accounted for. In order to do so, the aspect ratio AR is artificially increased by multiplication factor $K_{W(B)}$ which typically is chosen as 1.3 (Hoak and Finck, 1978; Graham and McDowell, 2008). The aspect ratio is calculated as follows for the semi-span (one free end) and full-span (two free ends):

$$\mathrm{AR} = \frac{\left(bK_{W(B)}\right)^2}{2A} \quad \text{(one free end)}, \tag{39}$$

$$\mathrm{AR} = \frac{\left(bK_{W(B)}\right)^2}{A} \quad \text{(two free ends)}. \tag{40}$$

The total drag of the control surfaces is the sum of profile drag and lift-induced drag. It again is assumed that skin friction dominates the profile drag, hence form drag is dismissed. The coefficient of total drag for control surfaces is

$$C_D = 2C_f + C_{Di}. \tag{41}$$

The skin friction coefficient is the same as in (28) with Reynolds number from (26), only the characteristic length changes to chord length of the control surface. Scaling by factor 2 is necessary since the reference area in (36) is the planform area, not the total wetted surface area. The induced drag coefficient is calculated as (Anderson Jr, 1985)

$$C_{Di} = \frac{C_L^2}{\pi e \mathrm{AR}}. \tag{42}$$

With (22)–(42) it is now possible to solve the governing set of Eqs. (17)–(19) in computer algebra software (e.g. Matlab®) and determine the resulting steady-state vehicle flight mechanics. The modular structure of this system of equations allows for simple implementation of external higher-fidelity data in the form of look-up tables, e.g. from experimental data from wind tunnel testing or numerical data from more sophisticated methods such as Vortex Lattice Method (VLM) or Computational Fluid Dynamics (CFD) software.

4. Transit efficiency of legacy gliders

Case studies on the hull shapes of the legacy gliders Slocum, Spray and Seaglider are performed with the goal of evaluating the transit efficiency of these vehicles in glider configuration and propeller configuration when operating in both ideal and biofouling conditions. The transit efficiency is evaluated by means of the glide metric (13) with the efficiency-ratio set to one. Several simplifications and assumptions are made in order to perform this case study:

- Most commercial propeller-driven AUVs are designed to have positive buoyancy and maintain submerged level flight through hydrodynamic lift (see e.g. McPhail (2009)). Some large-scale AUVs (Tangirala and Dzielski, 2007; Tiwari and Sharma, 2020) and highly-specialized AUVs such as hovering and hydrobatic AUVs (Bhat et al., 2019) use buoyancy systems to achieve neutral buoyancy, and few use a combination of both methods (Bi et al., 2020). In this study, it is assumed that the propeller-driven AUV can maintain level flight at no additional energy cost, i.e. the power component from actuation of either control surfaces (additional induced drag has to be overcome) or buoyancy system is neglected.
- It further is assumed that the size of the propeller powertrain equals the size of the buoyancy engine powertrain.
- In general, compressibility effects as well as buoyancy variations (ocean stratification) are neglected in this study. This assumption is required in order to keep the model at a reasonably complex level. Whether this assumption holds depends on the actual design of the underwater glider. Seaglider is designed to compress at the same rate as seawater, leading to constant buoyancy (Eriksen et al., 2001).
- The feasibility of buoyancy engine (BE) sizing is not assessed even though the forward velocity of underwater gliders is directly proportional to the magnitude of net buoyancy and hence size of the BE. Open, seawater-based systems provide significantly larger buoyancy changes than closed, oil-based systems.
- The ratio of propeller-train efficiency to VBS-efficiency is assumed to be 1. As mentioned in Section 2.2, there is a large variation of VBS-efficiency depending on operating conditions and technology. The introduced uncertainty is too large to be considered in this study.

4.1. Slocum and spray

The Slocum underwater glider is based on a idea of heat-exchange powered, buoyancy-driven underwater vehicles by Henry Stommel from 1989 (Stommel, 1989). It was developed in collaboration with Webb et al. (2001) and named after Joshua Slocum, the first human to solo circumnavigate the earth. As of today, the glider is commercially available in thermally and electrically powered vehicle configurations. Slocum's hull is of typical torpedo-like Myring shape. Scripps Institution of Oceanography has developed a similar underwater glider (only electrical) which is named after *Spray*, Joshua Slocum's sloop. In the typical range of operating Reynolds-number (1×10^5 to 1×10^6) the hydrodynamic coefficients can be considered constant with respect to Reynolds number (Sherman et al., 2001; Rudnick et al., 2004). Lift and drag coefficients have been determined numerically by Vehicle Control

Table 1
Polynomial coefficients for curve fitting of Seaglider drag and lift coefficients.

	R^2	p_{00}	p_{10}	p_{01}	p_{20}	p_{11}	p_{02}
C_D	95.81 %	0.1463	−0.2863	−0.001 387	0.2011	0 (fixed)	0.001 248
C_L	98.05 %	0 (fixed)	0 (fixed)	0.058 78	0 (fixed)	0.023 46	–

Technologies, Inc. (VCT). Here, the reader should be cautious and note that the reference area is the hull length squared, a convention taken over from VCT. The published coefficients (α in radians) read as follows for Slocum (Humphreys et al., 2003; Humphreys, 2003c)

$$C_D = 0.0015587\alpha^2 + 0.058202, \tag{43}$$

$$C_L = 0.13058\alpha^2 + 0.051143\alpha|\alpha|, \tag{44}$$

and for Spray (Humphreys et al., 2003; Humphreys, 2003a)

$$C_D = 0.0020406\alpha^2 + 0.044463, \tag{45}$$

$$C_L = 0.11878\alpha^2 + 0.038418\alpha|\alpha|. \tag{46}$$

Coefficients for Slocum for a wide range of angles of attack have also been determined experimentally in wind tunnel tests in the past (Berman, 2003). The data confirms the computed lift coefficient but shows significant deviations in drag coefficient, which are reported to likely be due to uncertainties in the processing of drag force measurements. However, the experimental data qualitatively supports the numerical data, increasing confidence levels therein. Since bare-hull coefficients are not available an empirical estimate for the wing drag is subtracted from the vehicle drag at zero angle of attack. Assuming that wing drag is governed by skin friction drag, (27) and (41) with the approximate wing dimensions from Rudnick et al. (2004) and Jenkins et al. (2003) are used for the drag reduction.

4.2. Seaglider

The commercial underwater glider Seaglider has been thoroughly investigated in the past by several researchers. The vehicle's design and main particulars are presented in Eriksen et al. (2001) and Rudnick et al. (2004). Seaglider's laminar flow-shape hull experiences significant *Re*-effects as previously reported e.g. by Sherman et al. (2001) and Rudnick et al. (2004). The coefficients published by VCT (Humphreys, 2003b; Humphreys et al., 2003) do not take into account Reynolds number effects and hence cannot be used in this study. Fortunately, an extensive data set of lift, drag and moment coefficients from full-scale wind tunnel tests with different vehicle configurations has been published in Techy et al. (2010). The reader should note that here volumetric hydrodynamic coefficients are used, i.e. the reference area is the square of the cube root of the body volume, i.e. $V^{2/3}$. For this study, the data has partly been digitized and post-processed. The data confirms the *Re*-effects and therefore physically sound solutions need to be determined numerically through regression in two dimensions, i.e. angle of attack and inflow velocity. In this study, the Matlab® Curve Fitting Tool is used to interpolate and extrapolate the drag and lift coefficients for different values of U and α. The drag coefficients and lift coefficients have been curve-fitted with a 2nd-order/2nd-order polynomial ($R^2 = 95.81\,\%$) and a 2nd-order/1st-order polynomial ($R^2 = 98.05\,\%$), respectively. The coefficients are shown in Table 1.

$$C_D = p_{00} + p_{10}U + p_{01}\alpha + p_{20}U^2 + p_{11}U\alpha + p_{02}\alpha^2 \tag{47}$$

$$C_L = p_{00} + p_{10}U + p_{01}\alpha + p_{20}U^2 + p_{11}U\alpha \tag{48}$$

Curve fitting enables evaluation of C_D and C_L at any given input value and application of a numerical nonlinear system solver for computation of the Re-corrected flight states. The bare hull drag coefficient at zero angle of attack can be approximated by a simple power function ($R^2 = 0.9839$) as (also see Fig. 3):

$$C_D = 0.034 \cdot U^{-0.55} \tag{49}$$

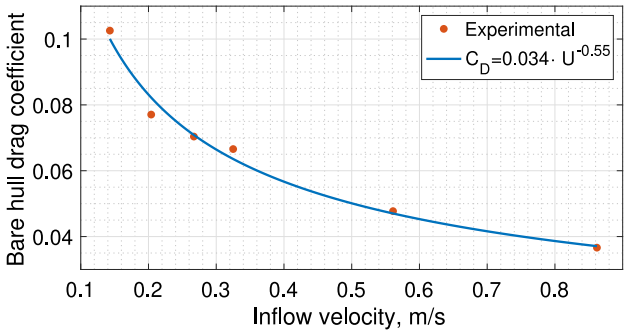

Fig. 3. Volumetric drag coefficient for the Seaglider hull without wings, based on Techy et al. (2010).

Due to the Reynolds number effects the optimum glide path angle also becomes dependent on *Re*, making the evaluation of (9) significantly more difficult. While for Slocum and Spray the transit performance can be evaluated by considering only a (constant) optimum angle of attack a wider range of angles of attack must be considered for Seaglider; the minimum energy consumption (lowest glide coefficient (12)) is then found numerically as the lower envelope for of the different levels of energy consumption in all possible flight states. Due to extrapolation uncertainties the presented results for Seaglider are only be considered reliable for the velocity range up to $0.862\,\mathrm{m\,s^{-1}}$, the highest velocity studied by Techy et al. (2010).

4.3. Transit performance

The transit performance of the legacy underwater gliders is evaluated in terms of the glide metric (13) for each configuration, i.e. underwater glider and propeller-modified vehicle. Biofouling conditions are considered by penalizing the hydrodynamic coefficients artificially as in (14) and (15) (according to Section 2.3). In order to correctly interpret the results, the reader is reminded that a glide metric lower than 1 indicates more energy-efficient horizontal travel of the underwater glider (compared to a propeller-driven AUV of the same shape); vice-versa, a glide metric greater than 1 means more energy-efficient horizontal travel of the propeller-driven AUV. A metric of value 1 means equally energy-efficient travel. These relations come from the division of the equivalent propulsive power of the glider by the propulsive power of the propeller-driven AUV leading to the glide metric (13). Fig. 4 shows the glide metric for all three vehicles in ideal conditions and in the presence of biofouling.

For the Slocum and Spray bodies with *Re*-independent hydrodynamic coefficients advantages for gliding locomotion in ideal conditions can be observed (25 % to 30 % lower power consumption), whereas in the presence of biofouling the propeller-configurations proves significantly more efficient (45 % to 50 %). Seaglider's transit performance is significantly influenced by *Re*-effects and tends to decrease with increasing velocity. For the ideal case, the glider configuration proves more efficient up to a horizontal velocity of $\approx 0.95\,\mathrm{m\,s^{-1}}$, where transit efficiency of both vehicle configurations is equal. This point already lies above the highest velocity studied by Techy et al. (2010); yet, a trend of rapidly decreasing glider performance can clearly be seen. For the biofouling case, as for the other two gliders, the propeller-driven version of the vehicle is more efficient throughout the considered velocity range (from 15 % to 300 % higher efficiency). Furthermore, the transit performance of Seaglider is subject to significant oscillations. These can be explained as follows: Both optimum angle of attack and glide coefficient C_{GL} can be approximated as functions of velocity squared within the velocity range of interest (with a minimum at $\approx 0.7\,\mathrm{m\,s^{-1}}$). As shown in Fig. 3, the bare-hull drag coefficient can be approximated by a power function. The observed oscillations in the results are caused

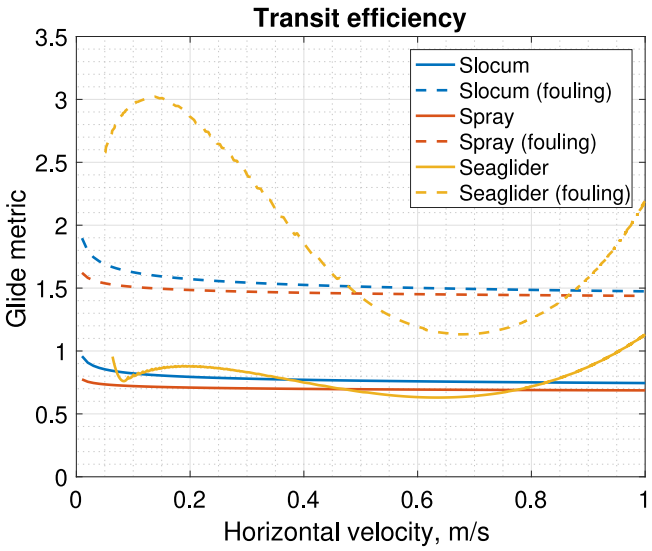

Fig. 4. Transit efficiency of the legacy underwater gliders expressed in terms of the glide metric.

by division of the glide coefficient (parabolic shape) by the bare hull drag coefficient (power function). The hydrodynamic reasons for this behaviour go beyond the scope of this paper. The effect of biofouling amplifies the observed oscillations.

The drastic decrease in glider transit performance when the vehicle is subject to biofouling is due to a double penalty in drag and lift, rendering propeller-driven AUVs more efficient than underwater gliders. Biofouling can be prevented or reduced by avoiding tropical and subtropical water masses as well as by operating in deep water and minimizing surfacing time. If long-endurance missions are to be conducted in biofouling-prone areas sufficient antifouling measures have to be taken and a propeller-driven AUV can be the vehicle type of choice. A further risk related to biofouling is the associated change in buoyancy and mass; an issue that has to be addressed in the future.

5. Model validation and application

It can be shown that the model presented in Section 3, predicts the hydrodynamic behaviour of underwater vehicles qualitatively correct within acceptable errors bounds. The model has been validated against the published Slocum data (Humphreys, 2003c; Humphreys et al., 2003) in the velocity range $0.1\,\mathrm{m\,s^{-1}}$ to $1\,\mathrm{m\,s^{-1}}$ (uniform increments of $0.1\,\mathrm{m\,s^{-1}}$) for angles of attack from 0° to 15° (uniform increments of 0.05°). The model input data is given in Table 2 and is based on the data published by Rudnick et al. (2004). Fig. 5a shows the glide polar for the Slocum hull using the published CFD data (continuous lines) and the presented model (dashed lines). The glide polar itself serves as a fairly good means of visualization of the related error since it contains information about both lift and drag at various angles of attack. Figs. 5b and 5c show the percentage error distribution for drag and lift forces. It can be seen that lift is modelled with satisfying accuracy throughout the model range with errors typically not exceeding ≈15 %. The empirical estimates for drag forces deviate from the published CFD data by up to ≈25 %. The presented model proves to be better at predicting lower velocities ($\leq 0.25\,\mathrm{m\,s^{-1}}$) and higher velocities ($0.75\,\mathrm{m\,s^{-1}}$), where the associated error mostly remains under 15 %. For medium velocities, the associated area tends to be slightly higher (mostly around 10 % to 20 %).

The steady-state flight mechanics model is now applied to the Slocum underwater vehicle in order to study the effects of wing size on vehicle performance. While the wing positioning only affects the requirements towards moving masses (ignoring changing interference

Table 2
Model Input: Slocum-like underwater vehicle.

Body	L	D	mg	x_b	z_b
	1.80 m	0.21 m	52 kg	0.9 m	0 m
	x_G	z_G	x_B	z_B	A_{wet}
	0.9 m	0 m	0.9 m	−0.01 m	1.19 m^2
Wings	N	c_w	b_w	x_w	z_w
	2	0.12 m	0.4 m	0.8 m	0 m
Vertical tail (drag only)	N	c_t	b_t	x_t	z_t
	1	0.15 m	0.18 m	−0.39 m	0 m

effects related to wing positioning), the actual wing span can be modified to optimize a glider's transit performance. Using the model input data from Table 2, the glide metric (13) (with reference drag coefficient C_{D0} being the body-only drag coefficient at zero angle of attack) is calculated for different wing configurations (aspect ratios). Different net buoyancies ranging from 1 N to 8 N are used, and the wing span is varied from 0 % to 250 % of the standard wing size. The results are shown in Fig. 6. The blue area shows the glide metric as computed band for each wing configuration at the resulting optimal flight state. The width of that band represents the range of achievable glide velocities. The results suggest that Slocum's actual wing span represents a near-optimum design, with the glide metric being close to a minimum at ≈100 % wing span. Both increasing and decreasing wing spans have adverse effects on transit performance.

6. Discussion

Evaluating the transit performance of underwater vehicles is an ambitious task and in order to keep model complexity at a reasonable level, several assumptions had to be made. It is of great importance to bear in mind these assumptions when analysing or interpreting results.

A known issue is the underestimation of skin friction drag which likely originates from a violated smooth-body assumption (Phillips et al., 2008), commonly made when applying both empirical or computational methods. In fact, the discrepancy between modelling approaches and experimental data can easily be accounted for by changing the respective expressions in the model, i.e. improving modelling of the frictional drag coefficient. In this study, the model is validated against the much higher-fidelity results from CFD computations. When validating against experimental data, empirical estimates for the frictional drag coefficients as presented in Gudmundsson (2014) (essentially based on Schlichting et al. (2016)) or in Phillips et al. (2017) can yield better results. The decision to validate against CFD data was necessary due to the lack of reliable, high quality experimental data. Data on the effects of biofouling, or in a broader sense the effects of surface roughness, on lift and drag properties at varying angles of attack are scarce and require further attention. Consideration of such effects has been proven to be important, offering potential for future research. Furthermore, due to the operational portfolio of underwater gliders, the transition between laminar and turbulent flow can play an important role. As mentioned in Section 3.1, the transition zone is difficult to capture using simple models and more work is required on this topic. The interested reader is referred to literature, e.g. Lidtke et al. (2019).

The study shows that for certain applications the less expensive lower-fidelity models can be very useful, e.g. for performance evaluation at the early design stage. For the design of controllers and manoeuvring simulations, higher-fidelity models are required which are also capable of considering nonlinearities introduced by e.g. waves and currents. Such models can be found e.g. in Thomasson and Woolsey (2013). For controller design for underwater gliders subject to environmental disturbances the reader is referred to Ullah et al. (2019). The effects of a moving atmosphere on soaring of birds have also been studied (both analytically and empirically) by Taylor et al. (2016),

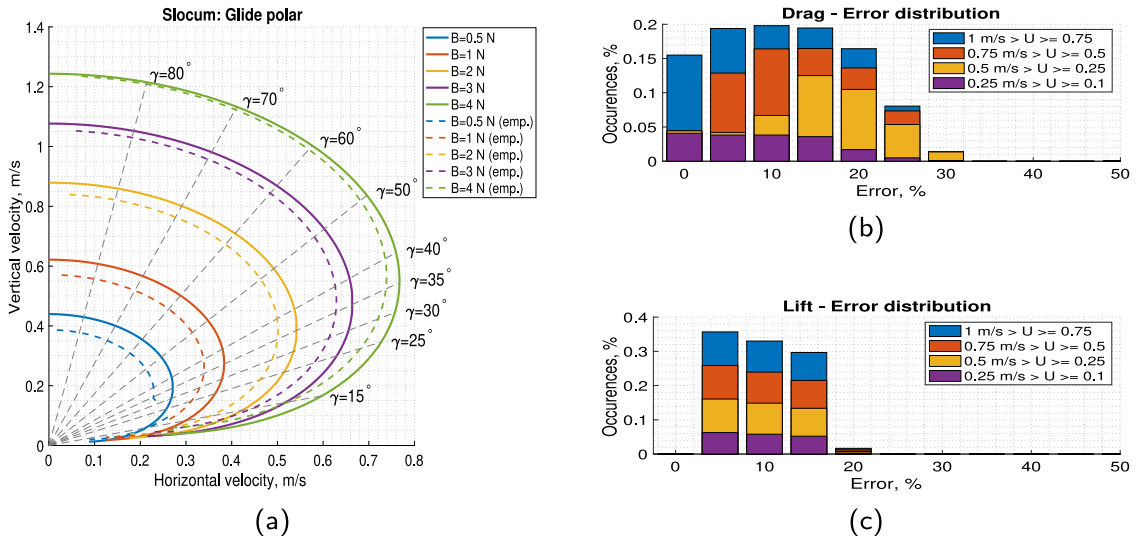

Fig. 5. Error analysis of the presented model compared to the solutions presented in (43) and (44) (Humphreys, 2003c). (a) The Slocum underwater glide polar based on the reference data (solid lines) compared to the output of the intermediate-fidelity model (dashed lines) for net buoyancies from 0.5 N to 8 N. (b) Percent error in drag. (c) Percent error in lift.

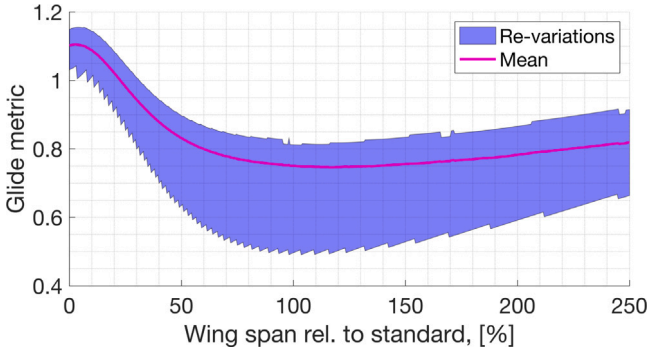

Fig. 6. The glide metric (13) for a Slocum-like design with varying wing span (relative to standard span) as calculated by the presented model.

who are suggesting that birds increase their airspeed in unfavourable headwinds and decrease their airspeed in favourable winds in order to minimize cost of transport. Further research on the applicability of such results to underwater robots is expected to yield interesting results.

Improving the performance of underwater vehicles is a popular topic among maritime and robotic researchers. There are many different approaches to solve this problem, including bio-inspired and biomimetic robots. Recent research on *body and/or caudal fin* (BCF) and *median and paired fins* (MPF) swimmers lead to the conclusion that bio-inspired AUV design can further improve the overall performance of AUVs (Scaradozzi et al., 2017). For future research, it will be interesting to extend the evaluation of AUV propulsion systems to include *new* means of locomotion (such as BCF and MPF). One difficulty that also arises with other propulsion systems are uncertainties in the powertrain efficiencies. As mentioned in Section 2.2, the powertrain efficiency for propellers are well known (potentially due to maturity of technology) whereas the efficiency of buoyancy systems can vary significantly. This may be understood as a call for further research on buoyancy systems and their implementation in underwater vehicles.

7. Conclusions

This paper contributes to answering the often disputed transit performance of underwater gliders in comparison to common propeller-driven AUVs by extending previous studies (e.g. Steinberg et al. (2010) and Dhanak and Xiros (2016)) in terms of operating conditions and speed. A simple but practical glide metric based on hydrodynamic coefficients is introduced and consequently used to compare the transit performance of the existing, state-of-the-art legacy underwater gliders to propeller-driven versions thereof. Mathematical evaluation of the left-hand side of the glide metric (13) shows that in the best-possible case (assume $C_L \gg C_D \approx C_{D0}$) the glider can be twice as efficient as the propeller-driven vehicle. In reality however, the reference drag coefficient of the unwinged vehicle at zero angle of attack can be significantly lower than the glider's drag coefficient, yielding higher glide metrics. For the legacy gliders Slocum and Spray this glide metric is about 0.75, indicating a 25 % higher efficiency for gliding locomotion. For the Seaglider hull, this glide metric fluctuates around the same value for velocities up to $0.8\,\mathrm{m\,s^{-1}}$ but experiences significantly adverse *Re*-effects for velocities $>0.8\,\mathrm{m\,s^{-1}}$. While these results are true for ideal operating conditions it is also found that the presence of biofouling inflicts a double-penalty on underwater gliders by increasing drag and decreasing lift. When biofouling is taken into account, propeller-driven vehicles generally show superior transit performance. As a result, the choice of propulsion method becomes not only a question of design but also operating conditions. The most significant demerits are the associated modelling uncertainties, in particular in the estimation of frictional drag, modelling of transitional flows and consideration of powertrain efficiencies.

Furthermore, a tool for the prediction of vehicle performance is provided in form of an intermediate-fidelity flight mechanics model. The model is validated against the published Slocum-data (Humphreys, 2003c) and it is shown that the vehicle performance is predicted qualitatively correct within acceptable error bounds (strictly $\lesssim$30 %). As an example, the model is demonstrated finding an optimum wing span that provides best transit performance; unsurprisingly, this optimal wing span is found to be the already existing one. The strengths of the intermediate-fidelity model lie in its simplicity and modularity, allowing not only for quick computation time but also implementation of external data sets from CFD studies or wind tunnel tests in the form of look-up tables. Also – if more-specific design parameters are known – more design-specific approximations for estimations of hull forces can be used, e.g. Jorgensen (1973b,a) and Hopkins (1951). For a detailed analysis of more complex flow phenomena such as interference between wings and hull as well as the flow around appendages like antennas and acoustic links, a thorough CFD-based approach however still is deemed unavoidable.

CRediT authorship contribution statement

Clemens Deutsch: Conceptualization, Data curation, Formal analysis, Investigation, Methodology, Project administration, Software, Validation, Visualization, Writing - original draft, Writing - review & editing. **Jakob Kuttenkeuler:** Conceptualization, Formal analysis, Funding acquisition, Methodology, Software, Supervision, Writing - original draft. **Tomas Melin:** Conceptualization, Formal analysis, Methodology, Writing - review & editing.

Declaration of competing interest

The authors declare that they have no known competing financial interests or personal relationships that could have appeared to influence the work reported in this paper.

Acknowledgements

This work was supported by Stiftelsen för Strategisk Forskning (SSF), Sweden through the Swedish Maritime Robotics Centre (SMaRC) (IRC15-0046).

References

Anderson Jr, J., 1985. Fundamentals of aerodynamics. Fundamentals of Aerodynamics, Volume Third Edit. McGraw-Hill, p. 982. http://dx.doi.org/10.1036/0072373350, URL http://scholar.google.com/scholar?hl=en&btnG=Search&q=intitle:Fundamentals+of+Aerodynamics#0.

Berman, S., 2003. Comparison of the Lift , Drag , and Pitch Moment Coefficients of a Slocum Glider Wind Tunnel Model with Computational Results. Princeton University.

Bhat, S., Stenius, I., Bore, N., Severholt, J., Ljung, C., Torroba Balmori, I., 2019. Towards a Cyber-Physical System for Hydrobatic AUVs. http://dx.doi.org/10.1109/oceanse.2019.8867392.

Bi, A., Zhao, F., Zhang, X., Ge, T., 2020. Combined depth control strategy for low-speed and long-range autonomous underwater vehicles. J. Mar. Sci. Eng. 8 (3), 181. http://dx.doi.org/10.3390/jmse8030181.

Chen, Y.J., Chen, H.X., Ma, Z., 2015. Hydrodynamic analyses of typical underwater gliders. J. Hydrodyn. 27 (4), 556–561. http://dx.doi.org/10.1016/S1001-6058(15)60516-9.

Dhanak, M.R., Xiros, N.I., 2016. Springer handbook of ocean engineering. Springer Handbook of Ocean Engineering. pp. 1–1345. http://dx.doi.org/10.1007/978-3-319-16649-0.

Eriksen, C.C., Osse, T.J., Light, R.D., Wen, T., Lehman, T.W., Sabin, P.L., Ballard, J.W., Chiodi, A.M., 2001. Seaglider: A long-range autonomous underwater vehicle for oceanographic research. IEEE J. Ocean. Eng. 26 (4), 424–436. http://dx.doi.org/10.1109/48.972073.

Fu, X., Lei, L., Yang, G., Li, B., 2018. Multi-objective shape optimization of autonomous underwater glider based on fast elitist non-dominated sorting genetic algorithm. Ocean Eng. 157, 339–349. http://dx.doi.org/10.1016/j.oceaneng.2018.03.055.

Furlong, M., McPhail, S., Stevenson, P., 2007. A concept design for an ultra-long-range survey class AUV. In: OCEANS 2007 - Europe. pp. 1–6. http://dx.doi.org/10.1109/OCEANSE.2007.4302453.

Furlong, M.E., Paxton, D., Stevenson, P., Pebody, M., McPhail, S.D., Perrett, J., 2012. Autosub long range: A long range deep diving AUV for ocean monitoring. In: 2012 IEEE/OES Autonomous Underwater Vehicles, AUV 2012. pp. 1–7. http://dx.doi.org/10.1109/AUV.2012.6380737.

Gafurov, S.A., Klochkov, E.V., 2015. Autonomous unmanned underwater vehicles development tendencies. In: Procedia Engineering. Elsevier, pp. 141–148. http://dx.doi.org/10.1016/j.proeng.2015.06.017.

Graham, R.E., McDowell, J.L., 2008. Simplification of the wing-body interference problem. J. Aircr. 9 (10), 752. http://dx.doi.org/10.2514/3.59073.

Gudmundsson, S., 2014. General aviation aircraft design. General Aviation Aircraft Design. Butterworth-Heinemann, pp. 661–760. http://dx.doi.org/10.1016/B978-0-12-397308-5.00015-5.

Haldeman, C.D., Aragon, D.K., Miles, T., Glenn, S.M., Ramos, A.G., 2016. Lessening biofouling on long-duration AUV flights: Behavior modifications and lessons learned. In: OCEANS 2016 MTS/IEEE Monterey, OCE 2016. http://dx.doi.org/10.1109/OCEANS.2016.7761236.

Hoak, D.E., Finck, R.D., 1978. USAF Stability and Control Datcom, Volume 2, Rev. ed. Global Engineering Documents, Irvine, CA.

Hobson, B.W., Bellingham, J.G., Kieft, B., McEwen, R., Godin, M., Zhang, Y., 2012. Tethys-class long range AUVs-extending the endurance of propeller-driven cruising AUVs from days to weeks. In: 2012 IEEE/OES Autonomous Underwater Vehicles, AUV 2012. http://dx.doi.org/10.1109/AUV.2012.6380735.

Hoerner, S.F., 1965. Fluid-Dynamic Drag: Practical Information on Aerodynamic Drag and Hydrodynamic Resistance. Hoerner, Brick Town, NJ.

Hopkins, E.J., 1951. A Semi-Empirical Method for Calculating the Pitching Moment of Bodies of Revolution at Low Mach Numbers. NACA RM A51C14, NACA, Washington.

Humphreys, D.E., 2003a. Validation of the Hydrodynamics & MAneuvering Model for the Scripps Institution of Oceanography Spray Glider. Technical Report, Vehicle Control Technologies, Inc., Reston VA, p. 27.

Humphreys, D.E., 2003b. Validation of the Hydrodynamics & Maneuvering Model for the University of Washington - APL Sea Glider. Technical Report, Vehicle Control Technologies, Inc., Reston VA, p. 38.

Humphreys, D.E., 2003c. Validation of the Hydrodynamics & Maneuvering Model for the Webb Research Corporation Slocum Glider. Technical Report, Vehicle Control Technologies, Inc., Reston VA, p. 26.

Humphreys, D., Osse, J., Jones, C., 2003. Validation of the hydrodynamic and manouvering models for three legacy undersea gliders. In: Proceedings of the 2003 International Symposium on Unmanned Untethered Submersible Technology. AUSI, New Hampshire.

Jenkins, S.A., Humphreys, D.E., Sherman, J., Osse, J., Jones, C., Leonard, N., Graver, J., Bachmayer, R., Clem, T., Carroll, P., Davis, P., Berry, J., Worley, P., Wasyl, J., 2003. Underwater Glider System Study. Technical Report, URL https://escholarship.org/uc/item/1c28t6bb.

Jorgensen, L.H., 1973a. A Method for Estimating Static Aerodynamic Characteristics for Slender Bodies of Circular and I Noncircular Cross Section Alone and with Lifting Surfaces at Angles of Attack from Oo TO 90". NASA TN D-7228, p. 39.

Jorgensen, L.H., 1973b. Prediction Aerodynamic of Static Characteristics for Space-Shuttle-Like and Other Bodies at Angles of Attack from 0° to 180°. NASA TN D-6996, pp. 1–12.

Joung, T.H., Sammut, K., He, F., Lee, S.K., 2012. Shape optimization of an autonomous underwater vehicle with a ducted propeller using computational fluid dynamics analysis. Int. J. Nav. Archit. Ocean Eng. 4 (1), 44–56. http://dx.doi.org/10.3744/JNAOE.2012.4.1.044.

Khor, Y.S., Xiao, Q., 2011. CFD simulations of the effects of fouling and antifouling. Ocean Eng. 38 (10), 1065–1079. http://dx.doi.org/10.1016/j.oceaneng.2011.03.004.

King, P., Williams, G., Coleman, R., Zurcher, K., Bowden-Floyd, I., Ronan, A., Kaminski, C., Laframboise, J.-M., McPhail, S., Wilkinson, J., Bowen, A., Dutrieux, P., Bose, N., Wahlin, A., Andersson, J., Boxall, P., Sherlock, M., Maki, T., 2019. Deploying an AUV beneath the Sørsdal Ice Shelf: Recommendations from an expert-panel workshop. In: 2018 IEEE/OES Autonomous Underwater Vehicle Workshop (AUV). Porto, pp. 1–6, http://dx.doi.org/10.1109/auv.2018.8729786.

Kobayashi, T., Asakawa, K., Watanabe, K., Ino, T., Amaike, K.I., Iwamiya, H., Tachikawa, M., Shikama, N., Mizuno, K., 2010. New buoyancy engine for autonomous vehicles observing deeper oceans. In: Proceedings of the International Offshore and Polar Engineering Conference, Vol. 2. pp. 401–405.

Lidtke, A.K., Turnock, S.R., Downes, J., 2019. Characterizing influence of transition to turbulence on the propulsive performance of underwater gliders. J. Ship Res. http://dx.doi.org/10.5957/JOSR.09180050.

Lobe, H., Haldeman, C., Glenn, S.M., 2010. ClearSignal coating controls biofouling on the rutgers glider crossing. Sea Technol. 51.

McPhail, S., 2009. Autosub6000: A deep diving long range AUV. J. Bionic Eng. 6 (1), 55–62. http://dx.doi.org/10.1016/S1672-6529(08)60095-5.

McPhail, S., Templeton, R., Pebody, M., Roper, D., Morrison, R., 2019. Autosub Long Range AUV Missions Under the Filchner and Ronne Ice Shelves in the Weddell Sea, Antarctica - an Engineering Perspective. In: OCEANS 2019 MTS/IEEE Marseille. Marseille.

Nahon, M., 1996. A simplified dynamics model for autonomous underwater vehicles. In: Proceedings of Symposium on Autonomous Underwater Vehicle Technology. pp. 373–379. http://dx.doi.org/10.1109/AUV.1996.532437.

Orme, J., Masters, I., Griffiths, R., 2001. Investigation of the effect of biofouling on the efficiency of marine current turbines. In: Proceedings of MAREC2001, International Conference on Marine Renewable Energies. Institute of Marine Engineers, London, pp. 91–99.

Phillips, A.B., Haroutunian, M., Man, S.K., Murphy, A.J., Boyd, S.W., Blake, J.I., Griffiths, G., 2012. Nature in engineering for monitoring the oceans: Comparison of the energetic costs of marine animals and AUVs. In: Further Advances in Unmanned Marine Vehicles. http://dx.doi.org/10.1049/PBCE077E{_}ch17.

Phillips, A.B., Haroutunian, M., Murphy, A.J., Boyd, S.W., Blake, J.I., Griffiths, G., 2017. Understanding the power requirements of autonomous underwater systems, Part I: An analytical model for optimum swimming speeds and cost of transport. Ocean Eng. 133, 271–279. http://dx.doi.org/10.1016/j.oceaneng.2015.12.014.

Phillips, A.B., Turnock, S.R., Furlong, M.E., 2008. Comparisons of CFD simulations and in-service data for the self propelled performance of an autonomous underwater vehicle. In: 27th Symposium on Naval Hydrodynamics. Seoul, South Korea.

Prandtl, L., 1925. Bericht über Untersuchungen zur ausgebildeten Turbulenz. Z. Angew. Math. Mech. (5), 136–139.

Roper, D.T., Phillips, A.B., Harris, C.A., Salavasidis, G., Pebody, M., Templeton, R., Amma, S.V.S., Smart, M., McPhail, S., 2017. Autosub long range 1500: An ultra-endurance AUV with 6000 Km range. In: OCEANS 2017 - Aberdeen, Vol. 2017-Octob. pp. 1–5. http://dx.doi.org/10.1109/OCEANSE.2017.8084928.

Rudnick, D.L., Davis, R.E., Eriksen, C.C., Fratantoni, D.M., Perry, M.J., 2004. Underwater gliders for ocean research. Mar. Technol. Soc. J. 38 (2), 73–84. http://dx.doi.org/10.4031/002533204787522703.

Sadraey, M.H., 2017. Aircraft performance: An engineering approach. Aircraft Performance: An Engineering Approach. CRC Press, p. 570. http://dx.doi.org/10.1201/9781315366913.

Scaradozzi, D., Palmieri, G., Costa, D., Pinelli, A., 2017. BCF swimming locomotion for autonomous underwater robots: a review and a novel solution to improve control and efficiency. Ocean Eng. 130, 437–453. http://dx.doi.org/10.1016/j.oceaneng.2016.11.055.

Schlichting, H., Gersten, K., Schlichting, H., Gersten, K., 2016. Fundamentals of Boundary–Layer Theory. In: Boundary-Layer Theory. pp. 29–49. http://dx.doi.org/10.1007/978-3-662-52919-5{_}2.

Sherman, J., Davis, R.E., Owens, W.B., Valdes, J., 2001. The autonomous underwater glider "Spray". IEEE J. Ocean. Eng. 26 (4), 437–446. http://dx.doi.org/10.1109/48.972076.

Steinberg, D., Bender, A., Friedman, A., Jakuba, M., Pizarro, O., Williams, S., 2010. Analysis of propulsion methods for long-range AUVs. Mar. Technol. Soc. J. http://dx.doi.org/10.4031/MTSJ.44.2.3.

Stommel, H., 1989. The slocum mission. Oceanography 2 (1), 22–25. http://dx.doi.org/10.5670/oceanog.1989.26, URL https://tos.org/oceanography/article/the-slocum-mission.

Tangirala, S., Dzielski, J., 2007. A variable buoyancy control system for a large AUV. IEEE J. Ocean. Eng. 32 (4), 762–771. http://dx.doi.org/10.1109/JOE.2007.911596.

Taylor, G.K., Reynolds, K.V., Thomas, A.L., 2016. Soaring energetics and glide performance in a moving atmosphere. Philos. Trans. R. Soc. B 371 (1704), http://dx.doi.org/10.1098/rstb.2015.0398.

Techy, L., Tomokiyo, R., Quenzer, J., Beauchamp, T., Morgansen, K., 2010. Full-Scale Wind Tunnel Study of the Seaglider Underwater Glider. Technical Report, Washington, p. 34.

Thomasson, P.G., Woolsey, C.A., 2013. Vehicle motion in currents. IEEE J. Ocean. Eng. http://dx.doi.org/10.1109/JOE.2013.2238054.

Tiwari, B.K., Sharma, R., 2020. Design and analysis of a variable buoyancy system for efficient hovering control of underwater vehicles with state feedback controller. J. Mar. Sci. Eng. 8 (4), 263. http://dx.doi.org/10.3390/jmse8040263.

Torenbeek, E., Wittenberg, H., 2009. Flight physics: Essentials of aeronautical disciplines and technology, with historical notes. Flight Physics: Essentials of Aeronautical Disciplines and Technology, with Historical Notes. Springer Netherlands, pp. 1–535. http://dx.doi.org/10.1007/978-1-4020-8664-9.

Ullah, B., Ovinis, M., Baharom, M.B., Ali, S.S.A., Khan, B., Javaid, M.Y., 2019. Effect of waves and current on motion control of underwater gliders. J. Mar. Sci. Technol. (Japan) http://dx.doi.org/10.1007/s00773-019-00660-1.

Wagner, J.F., 2003. Identifying the speed Polar during normal soaring flight. In: IUTAM Symposium on Identification of Mechanical Systems. Wuppertal, http://dx.doi.org/10.13140/RG.2.2.22321.58724.

Walker, J.M., Flack, K.A., Lust, E.E., Schultz, M.P., Luznik, L., 2014. Experimental and numerical studies of blade roughness and fouling on marine current turbine performance. Renew. Energy http://dx.doi.org/10.1016/j.renene.2013.12.012.

Webb, D.C., Simonetti, P.J., Jones, C.P., 2001. SLOCUM: An underwater glider propelled by environmental energy. IEEE J. Ocean. Eng. 26 (4), 447–452. http://dx.doi.org/10.1109/48.972077.

Worall, M., Jamieson, A.J., Holford, A., Neilson, R.D., Player, M., Bagley, P.M., 2007. A variable buoyancy system for deep ocean vehicles. In: OCEANS 2007 - Europe.

Yamagata, H., Maki, T., Yoshida, H., Nogi, Y., 2019. Hardware design of variable and compact AUV 'MONACA' for under-ice survey of antarctica. In: 2019 IEEE International Underwater Technology Symposium, UT 2019 - Proceedings. http://dx.doi.org/10.1109/UT.2019.8734395.

Yuh, J., Marani, G., Blidberg, D.R., 2011. Applications of marine robotic vehicles. Intell. Serv. Robot. 4 (4), 221–231. http://dx.doi.org/10.1007/s11370-011-0096-5.